

On the Interaction of Methyl Azide (CH_3N_3) Ices with Ionizing Radiation: Formation of Methanimine (CH_2NH), Hydrogen Cyanide (HCN), and Hydrogen Isocyanide (HNC)[†]

Alfredo Quinto-Hernandez and Alec M. Wodtke

Department of Chemistry and Biochemistry, University of California, Santa Barbara, Santa Barbara, California 93106, United States

Chris J. Bennett,[‡] Y. Seol Kim, and Ralf I. Kaiser*

Department of Chemistry, University of Hawaii at Manoa, Honolulu, Hawaii 96822, United States

Received: April 4, 2010; Revised Manuscript Received: November 18, 2010

Methyl azide (CH_3N_3) might be a potential precursor in the synthesis of prebiotic molecules via nonequilibrium reactions on interstellar ices initiated by energetic galactic cosmic rays (GCR) and photons. Here, we investigate the effects of energetic electrons as formed in the track of cosmic ray particles and 193 nm photons with solid methyl azide at 10 K and the inherent formation of methanimine (CH_2NH), hydrogen cyanide (HCN), and hydrogen isocyanide (HNC). We present a systematic kinetic study and outline feasible reaction pathways to these molecules. These processes might be also important in solar system analogue ices.

Introduction

Methyl azide (CH_3N_3) is an organic compound suggested to be present in Titan's atmosphere.¹ To date, the Voyager Infrared Radiometer and Infrared Spectrometer (IRIS) covering the near- to the far-infrared (IR) regions of the electromagnetic spectrum provided the only attempts to detect methyl azide on Titan.^{2,3} Some laboratory studies have explored the chemistry of methyl azide on Saturn's moon. On the basis of a continuous-flow plasma discharge simulation, Thompson et al.⁴ proposed that CH_3N_3 should be present as a trace constituent in Titan's stratosphere. This suggestion was also supported by Raulin et al.³ and Khelifi et al.;⁵ in both works, upper concentrations of methyl azide in Titan's atmosphere of about 1.5 and 5.4 ppb were calculated, respectively. Possible synthesis of methyl azide molecules can occur within the methane (CH_4) clouds in Titan's troposphere. The analysis of in situ data from Cassini–Huygens,^{6,7} in agreement with theoretical work,^{8,9} suggests that layered methane clouds are located in Titan's troposphere, an upper CH_4 ice cloud of between about 20 and 30 km and a lower liquid $\text{CH}_4\text{--N}_2$ cloud between ~8 and 16 km.^{10,11} Regarding the cloud gap, laboratory investigations mimicking Titan's troposphere¹² were carried out on a low-temperature (78–82 K) gas cell. This work suggested that in the cloud gap, solid CH_4 aerosol particles with a nitrogen (N_2) content of ~14% are present at about 19 km. Considering the low temperature at this altitude (~78 K¹³) and that energetic cosmic rays can penetrate deep into the lower atmospheric layers,^{14,15} simple organic reactions involving methane and nitrogen ice mixtures are expected to be observed. These particles can interact with ionizing irradiation slightly higher than $4.5 \times 10^9 \text{ eV cm}^{-2} \text{ s}^{-1}$, the GCR flux estimated by Molina-Cuberos et al.¹⁶ to be

deposited on the Titan's surface. Recently, Jamieson et al.¹⁷ identified an absorption band centered at 2128 cm^{-1} in IR spectra obtained from methane and nitrogen ice mixtures exposed to energetic electrons in astrophysical conditions, which may correspond to the strong asymmetric stretch NNN of methyl azide. If that is true, traces of methyl azide should be synthesized also on Titan, likely occurring efficiently enough to explain the low concentrations predicted as upper limits by Raulin et al.³ and Khelifi et al.⁵

With this in mind, it is of interest to undertake studies of the chemistry of methyl azide ices, the subject of this work. Once methyl azide is decomposed, possible products are methanimine (CH_2NH), hydrogen cyanide (HCN), and hydrogen isocyanide (HNC), widely known for their astrophysical importance. The CH_2NH molecule has been detected in the interstellar medium^{18–20} and in ices in the comet C/1995 O1 (Hale–Bopp),²¹ and its presence has been suggested in the icy surfaces of Pluto and Triton (Neptune's largest moon)²² and in Titan's upper atmosphere.²³ HCN and HNC are seen in the gas phase in the interstellar medium,^{24,25} cometary comae,^{26–29} and Titan.⁶ Several studies have suggested that the astrophysical fate of CH_2NH on ices exposed to ionizing irradiation is to dissociate to HCN and HNC.^{22,28} In astrobiology, all of these molecules are thought to have a significant role in the synthesis of prebiotic molecules. For example, it has been reported that CH_2NH could react either with HCN or HNC in interstellar ice particles to produce aminoacetonitrile,^{30,31} a precursor of glycine.

Considering laboratory studies of methyl azide decomposition in the solid state, the experimental work has been limited to identifying its products after photolysis. In the early study of Milligan,³² the IR spectrum of methyl azide was recorded in argon matrix-isolated ice at 4.2 K and in carbon dioxide ice at 50 K. After photolysis, absorption bands of CH_2NH and HCN were observed. Also through photolysis of ice samples of methyl azide, Jacox and Milligan obtained the

[†] Originally submitted for the "Reinhard Schinke Festschrift", published as the September 16, 2010, issue of J. Phys. Chem. A (Vol. 114, No. 36).

* To whom correspondence should be addressed. E-mail: ralfk@hawaii.edu.

[‡] Also at NASA Astrobiology Institute, University of Hawaii at Manoa, Honolulu, HI 96822.

complete IR spectrum of CH₂NH³³ and HNC.^{34,35} In the same track, Jacox and Milligan concluded that HNC should be produced through the secondary photodissociation of CH₂NH³⁴ or from a rapid isomerization of HCN.³⁵ Also, Ferrante³⁶ detected triplet methylnitrene (³CH₃N) via UV absorption spectroscopy in the photolysis of samples of methyl azide and metastable molecular nitrogen trapped in solid nitrogen at 10 K, re-examining the previous identification of ³CH₃N by Barash et al.³⁷ Ferrante's work tends to confirm the assignment of ³CH₃N made by Carrick and Engelking³⁸ in their gas-phase emission study.

Despite the literature described above, there is a conspicuous lack of experimental evidence on well-defined reaction pathways, mechanistic studies, and quantitative rate constants of the CH₃N₃ decomposition to CH₂NH and subsequently to HCN and HNC in low-temperature ices with relevance to our solar system. Here, we present a systematic investigation designed to understand the dissociation mechanisms of methyl azide and CH₂NH in low-temperature ices by energetic electrons and by UV photons. Because CH₂NH is a potential candidate to understand the origin of HCN and HNC in astrophysical bodies and all of them are important precursors for possible pathways to larger organic molecules such as aminoacetonitrile,^{30,31} these studies could have significant implications for the organic chemistry in solar system ice analogues and its astrobiological evolution.

Experimental Methods

Methyl azide was synthesized through the reaction of solutions of sodium azide (5.5 mol %) and methyl *p*-toluenesulphonate (12.8 mol %) in anhydrous dimethylsulfoxide (DMSO) in a homemade two-chamber glass reactor following a procedure adapted from that reported by Khelifi et al.⁵ After placing and degassing (<1 mTorr) the solutions separately in each chamber of the reactor at room temperature, both solutions were mixed and then frozen at 77 K with liquid nitrogen (LN). The mixture was allowed to warm to room temperature; during the warm-up phase, methyl azide gas was obtained. The gas was transferred from the reactor to a glass tube submerged in LN through a cold trap (salty ice at 268 K) to avoid contamination. CH₃N₃ was collected as a brilliant white powder on the inner walls of the LN-cooled glass tube. The sample melted immediately once warmed to room temperature. After the collection of methyl azide, the system was degassed twice. We confirmed the purity of these samples through ¹H NMR.³⁹ The NMR spectra obtained showed methyl azide and traces of unidentified impurities.

The experiments were carried out in an ultrahigh vacuum (UHV) chamber evacuated to <5 × 10⁻¹¹ Torr through the use of oil-free magnetically suspended turbomolecular pumps.^{40,41} A polished silver mirror, located in the center of the chamber, served as a substrate onto which ices were condensed at 11.0 ± 0.4 K. In the electron irradiation experiments, methyl azide and 9 and 3% mixtures in nitrogen and argon, correspondingly, were condensed for 20 min at a pressure in the main chamber of 1 × 10⁻⁷ Torr on the silver target. The IR spectra of the samples were recorded using a Nicolet 6700 Fourier transform infrared (FTIR) spectrometer at a resolution of 2 cm⁻¹ in a range of 6000–500 cm⁻¹. The IR spectra of the ices were recorded on line and in situ prior to irradiation and in 2 min intervals during irradiation. Column densities were calculated following the work of Bennett et al.⁴⁰ The absolute band intensities of all detected

species were used as input to the Lambert–Beer relationship to obtain column densities, where IR absorption strengths were computed employing the hybrid density functional B3LYP method^{42,43} with the 6-311G(d, p) basis functions. All calculations were carried out using the GAMESS program.⁴⁴ Thus, the column densities of methyl azide samples prior to irradiation were found to be about 33 × 10¹⁶, 7.6 × 10¹⁶, and 2.6 × 10¹⁶ molecules cm⁻² for pure methyl azide, nitrogen, and argon matrix-isolated ices, respectively. For radiolysis studies, the samples were exposed at 11.0 ± 0.4 K to 5 keV electrons over 1 h while the chamber was held at about 1 × 10⁻¹⁰ Torr. The electron gun was operated at a nominal beam current of 100 nA with an extraction efficiency of about 78.8%. The expected number of electrons to hit the samples during the experiment was 78.8 nA (3600 s) = 4.90 × 10¹¹ electrons s⁻¹ (3600 s) = 1.8 × 10¹⁵, or 5.9 × 10¹⁴ electrons cm⁻² by scanning the electron beam over an area of 3.0 ± 0.4 cm². After completion of the radiation, the samples were warmed at a rate of 0.5 K min⁻¹ to 300 K.

For the photolysis experiments, we prepared samples of methyl azide ice and their respective matrix-isolated ices in argon (mixing ratio of 2.6%), nitrogen, and xenon (mixing ratio of 0.5%) and photolyzed them at 193 nm using a LAMBDA PHYSIK COMPex 110 excimer laser. These samples were prepared by condensation over 10 min at 11.0 ± 0.4 K at a pressure in the main chamber of 1 × 10⁻⁷ Torr. The column density of methyl azide ice and those in nitrogen, argon, and xenon matrix-isolated ices were calculated to be 29 × 10¹⁶, 4.2 × 10¹⁶, 2.6 × 10¹⁶, and 2.5 × 10¹⁶ molecules cm⁻², respectively. The samples were then exposed isothermally (11.0 ± 0.4 K) to a 193 nm laser beam during 30 min using a 10 Hz repetition rate and 9.5 mJ pulse energy (9.2 × 10¹⁶ photons s⁻¹) with a laser spot of 10 mm × 4 mm, that is, the expected number of photons to hit the samples at the end of the experiment was 1.66 × 10²⁰ photons or 4.15 × 10²⁰ photons cm⁻². Once the photon irradiation was stopped, these samples were warmed at a rate of 0.5 K min⁻¹ until they reached 300 K.

Results

The effects of the electron irradiation and the laser photolysis on the low-temperature samples were analyzed as follows. First, we inspected qualitatively the absorption bands of methyl azide (CH₃N₃) and assigned the carriers of the newly emerging absorption features during the irradiation and photolysis. Then, we plotted the temporal profiles of the column densities of the new absorptions. Finally, these data were fit to kinetic models to determine the rate constants of the decomposition of methyl azide and the production rates of the newly formed compounds during the electron irradiation and photolysis.

1. Qualitative Analysis. The IR spectroscopy of methyl azide has been extensively studied theoretically,^{45–47} recorded in the gas phase,^{5,48,49} and measured in matrix-isolated ices.³² On the basis of these literature data, we assigned all fundamentals of methyl azide in the spectral window of our FTIR spectrometer (6000–500 cm⁻¹) in the pure methyl azide ice and in the matrix-isolated samples (Figure 1; Table 1). We were also able to observe the combination bands $\nu_3 + \nu_6$, $2\nu_{12}$, $\nu_5 + \nu_{12}$, $2\nu_6$, and $2\nu_{13}$. These data are in excellent agreement with previous experimental studies of methyl azide.^{5,32,48,49}

IR spectra of the molecules formed after electron irradiation at 11 K are shown in Figure 2; a complete list of the

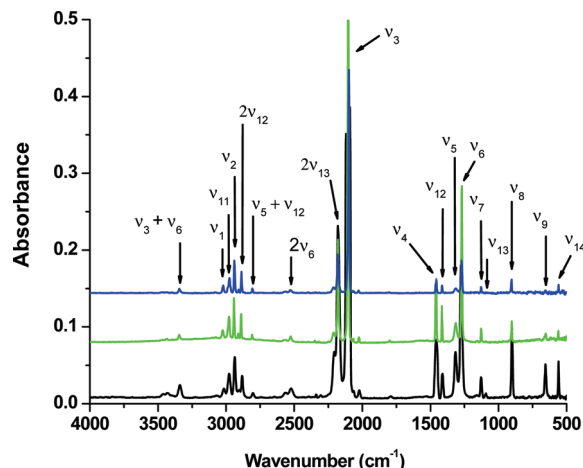


Figure 1. IR spectra of pure methyl azide (CH_3N_3) (black line), 9% methyl azide in a nitrogen matrix (green line), and 3% methyl azide in an argon matrix recorded at 10 K. The band positions are compiled in Table 1.

newly formed species and their assigned frequencies is provided in Table 2. In the neat methyl azide ice, we observed a reduction of all absorption bands and the formation of a new absorption at 1637 cm^{-1} ; this was identified as the ν_4 stretching vibration of CH_2NH . We were unable to observe any other molecules in this experiment. CH_2NH was also detected in the irradiated nitrogen and argon matrix-isolated ices via both the ν_4 and ν_6 fundamentals centered at 1637 and 1346 cm^{-1} in the nitrogen ice and 1639 and 1348 cm^{-1} in the argon ice. These wavenumbers agree well with previous observations.^{32,33,50,51} In the matrix-isolated ices, we also monitored HCN and HNC. HCN was detected by its intense ν_1 absorption centered at 3284 and 3300 cm^{-1} in the nitrogen and argon ices, respectively. These positions agree well with those observed in previous matrix isolation studies by King and Nixon,⁵² Gerakines et al.,⁵³ and Moore and Hudson.²² The less intense ν_2 mode at 746 cm^{-1} was not detected; the ν_3 vibrational mode reported by King and Nixon⁵² at about 2097 cm^{-1} was obscured by the ν_3 mode (NNN antisymmetric stretch) of CH_3N_3 . HNC was identified by its band centered at 3562 cm^{-1} in the nitrogen matrix-isolated ice and at 3581

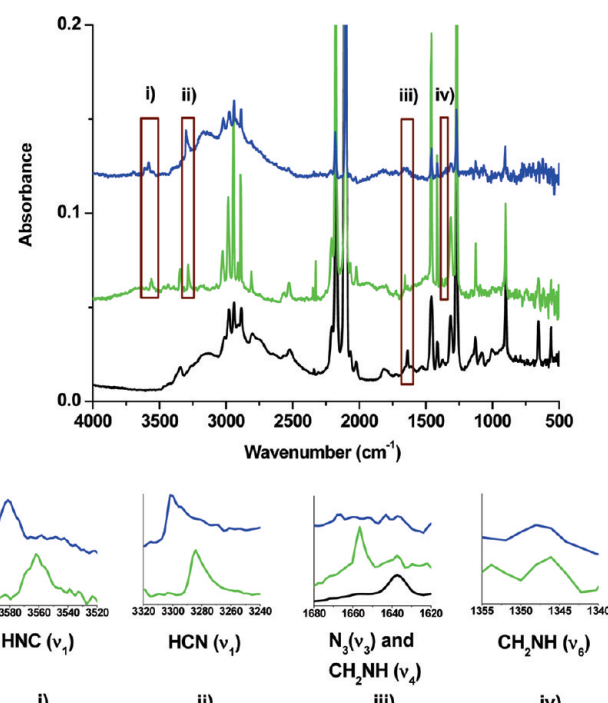


Figure 2. IR spectra of samples taken after 1 h of the irradiation of the pure methyl azide (black line), nitrogen (green line), and argon matrix-isolated ices with energetic electrons. The insets depict magnified views of the new absorption bands, (i) HNC (ν_1), (ii) HCN (ν_1), (iii) N_3 (ν_3) and CH_2NH (ν_4), and (iv) CH_2NH (ν_6). The band positions are compiled in Table 2.

TABLE 2: New IR Absorptions Observed in the Electron-Irradiated Samples at 10 K

species mode	band position (cm^{-1})				literature	
	pure	N_2	Ar	ref 5	ref 45	ref 48
CH_2NH	ν_4	1637	1637	1639	1638	C=N str
	ν_6	—	1346	1348	1342	HCN def
HCN	ν_1	—	3284	3300	—	3286
HNC	ν_1	—	3562	3581	—	3565
N_3	ν_3	—	1657	—	—	1657

cm^{-1} in argon. This feature was assigned to the ν_1 stretching vibration, reported previously at 3583 cm^{-1} by Milligan and

TABLE 1: Observed IR Absorptions of Methyl Azide (CH_3N_3) Recorded at 10 K in Pure and Matrix-Isolated Samples before the Electron Irradiation

mode	band position (cm^{-1})			literature			assignment
	pure	N_2	Ar	ref 5	ref 45	ref 48	
ν_1	3016	3023	3018	2818–2805	3023	3000	CH_3 antisym str
ν_2	2936	2941	2939	2119–2104	2935	2931	CH_3 sym str
ν_3	2092	2103	2103	2119–2104	2106	2143	NNN antisym str
ν_4	1457	1457	1457	1456–1450	1463	1482	CH_3 antisym def
ν_5	1319	1315	1315	1426–1407	1417	1351	CH_3 sym def
ν_6	1276	1269	1270	1284–1265	1272	1295	NNN sym str
ν_7	1128	1127	1128	1139–1119	1132	1118	CH_3 rock
ν_8	901	903	903	920–903	910	911	CN stretch
ν_9	655	660	656	676–658	666	654	NNN bend
ν_{10}	—	—	—	249	245	259	CNN bend
ν_{11}	2977	2977	2972	2940	2962	3000	CH_3 antisym str
ν_{12}	1417	1415	1413	1466	1463	1431	CH_3 antisym def
ν_{13}	1091	1093	1093	—	1103	1194	CH_3 rock
ν_{14}	559	560	—	561	560	790	NNN bend
ν_{15}	—	—	—		126		CH_3 torsion
$\nu_3 + \nu_6$	3340	3340	3343			3336	combination band
$2\nu_{12}$	2882	2886	2886			2884	combination band
$\nu_5 + \nu_{12}$	2804	2803	2804			2799	combination band
$2\nu_6$	2525	2523	2525	2539		2520	combination band
$2\nu_{13}$	2179	2179	2179	2198–2183			combination band

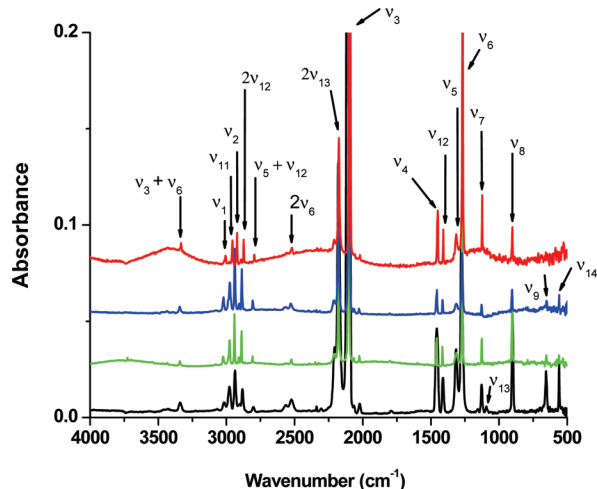


Figure 3. IR spectra of the pure methyl azide (CH_3N_3) (black line) and 0.5% methyl azide in a nitrogen matrix (green line), 2.6% methyl azide (CH_3N_3) in an argon matrix (blue line), and 0.5% methyl azide in a xenon matrix recorded at 10 K. The band positions are compiled in Table 3.

Jacox³⁴ and at 3565 cm^{-1} by Moore and Hudson.²² The reported ν_2 absorption mode at 477 cm^{-1} ^{35,54} is out of the spectral window of our detector. An additional band observed exclusively in the nitrogen ice was centered at 1657 cm^{-1} . This band was attributed to the ν_3 vibrational mode of the azide radical (N_3), which was also observed in previous works of electron bombardment in nitrogen ices.^{55,56} In Figure 3, we present the IR spectra of neat methyl azide ice as well as the spectrum obtained from methyl azide in the nitrogen, argon, and xenon matrix-isolated samples prior to photolysis at 193 nm. Table 3 summarizes the band assignments.

TABLE 3: Observed IR Absorptions of Methyl Azide (CH_3N_3) Recorded at 10 K in Pure and Matrix-Isolated Ices before the Photolysis at 193 nm^a

Mode	This Work				literature				Assignment	
	pure	N_2	Ar	Xe	$A(\nu) \times 10^{-18}$ ($\text{cm}^{-1}\text{ molec}^{-1}$)	band position (cm^{-1})	ref 5	ref 45	ref 48	
ν_1	3015	3023	3022	3006	2.46		3023	3000		CH_3 antisym str
ν_2	2937	2940	2939	2921	6.84	2818–2805	2935	2931	0.82 ± 0.03	CH_3 sym str
ν_3	2118	2098	2094	2094	79.33	2119–2104	2106	2143	60.1 ± 7.5	NNN antisym str
ν_4	1457	1456	1456	1450	3.3	1456–1450	1463	1482	0.59 ± 0.02	CH_3 antisym def
ν_5	1316	1313	1315	1315	1.29	1426–1407	1417	1351	1.58 ± 0.10	CH_3 sym def
ν_6	1276	1269	1270	1267	19.78	1284–1265	1272	1295	17.25 ± 0.55	NNN sym str
ν_7	1128	1126	1128	1124	1.68	1139–1119	1132	1118	1.20 ± 0.04	CH_3 rock
ν_8	902	903	904	902	3.17	920–903	910	911	2.65 ± 0.08	CN str
ν_9	656	653	651	—	1.80	676–658	666	654	1.46 ± 0.04	NNN bend
ν_{10}	—	—	—	—	1.08	249	245	259	0.36 ± 0.01	CNN bend
ν_{11}	2978	2975	2975	2956	8.80	2940	2962	3000	12.0 ± 0.5	CH_3 antisym str
ν_{12}	1412	1415	1415	1409	1.44	1460	1463	1431	0.68 ± 0.02	CH_3 antisym def
ν_{13}	1193	—	—	—	0.03		1103	1194		CH_3 rock
ν_{14}	560	560	559	561	2.00	561	560	790	0.68 ± 0.02	NNN bend
ν_{15}	—	—	—	—	0.50		126			CH_3 torsion
$\nu_3 + \nu_6$	3338	3342	3344	3332	—			3336		combination band
$2\nu_{12}$	2882	2888	2886	2873	—			2884		combination band
$\nu_5 + \nu_{12}$	2803	2807	2807	2796	—			2799		combination band
$2\nu_6$	2521	2524	2528	2520	—	2539		2520	1.62 ± 0.06	combination band
$2\nu_{13}$	2180	2179	2181	2175	15.80	2198–2183			17.7 ± 0.5	combination band

^a $A(\nu)$ is the integral absorption coefficient, defined as the absorption cross section over the range of wavenumbers where the ν absorption is significant, in $\text{cm}^{-1}\text{ molec}^{-1}$.

Figure 4 shows similar results after photolysis of methyl azide at 193 nm. As in the electron irradiation experiments, we identified only production of CH_2NH in the neat CH_3N_3 ice sample and CH_2NH , HCN, and HNC in the matrix ices (Table 4). CH_2NH was detected through six fundamental absorptions (ν_2 , ν_3 , ν_4 , ν_5 , ν_6 , and ν_7), and all of these peak positions were in excellent agreement with literature values.^{32,33,50,51} HCN and HNC were also positively identified; HCN was also detected via the CH stretch (ν_1) and bend (ν_2) modes, and HNC was detected through the NH stretch (ν_1) absorption. The N_3 radical could not be detected after photolysis in nitrogen solid, confirming the reports of Hudson and Moore.⁵⁷ Finally, the IR spectra of all of our samples after irradiation illustrate that CH_3N_3 or its photoproducts potentially formed several other species, but they were difficult to identify and quantify because their absorption bands either were broad or mixed with other ones, mainly observed in the region of 3500 – 2300 cm^{-1} .

2. Quantitative Analysis. The column densities of the methyl azide as well as the photoproducts were calculated using the strongest absorptions of each molecule observed during the course of our experiments. To monitor the evolution of the column density of CH_3N_3 , we used the integral absorption coefficient $A(\nu_3)$ or $A(2\nu_{13})$ shown in Table 3 for the absorption bands ν_3 or $2\nu_{13}$; for CH_2NH , $A(\nu_4)$ or $A(\nu_6)$ was used; for HCN, $A(\nu_1)$ was used; for HNC, $A(\nu_1)$ was used (shown in Table 4), and for N_3 , $A(\nu_3) = 4.00 \times 10^{-17}\text{ cm molecule}^{-1}$.⁵⁶ When pertinent, the column densities of the absorption bands in the species shown in Tables 1–4 were also obtained and used to calculate the error bars shown in Figures 5–10.

In the electron irradiation experiments, the column density of CH_3N_3 in the pure sample (Figure 5) decreased almost linearly after 1 h of exposure from $(33 \pm 10) \times 10^{16}$ to $(15$

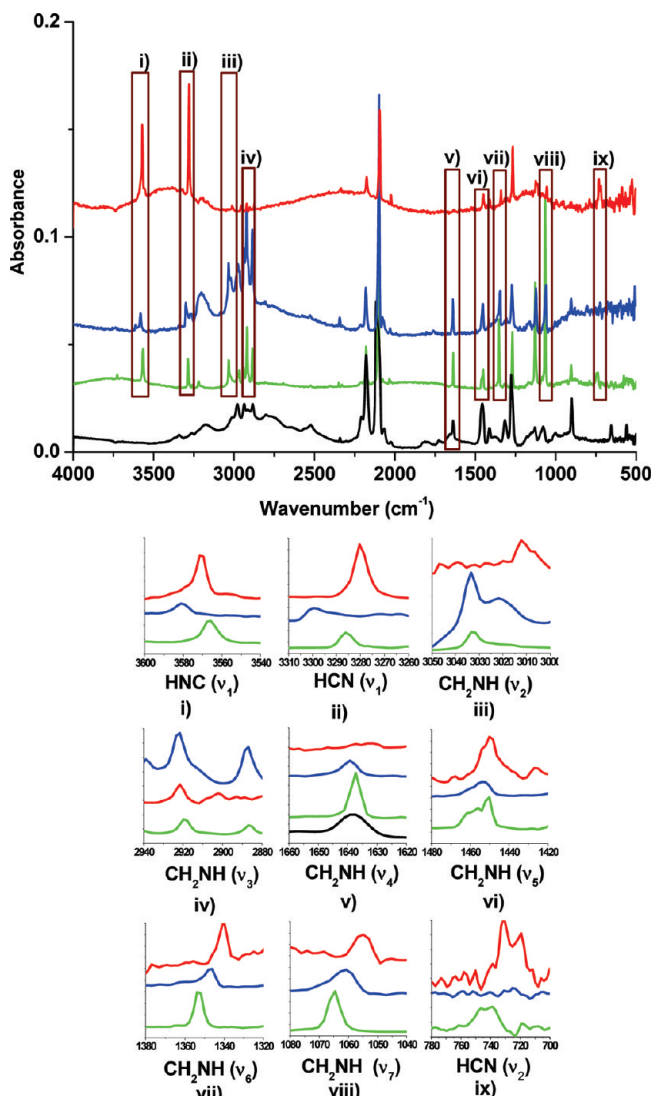


Figure 4. IR spectra of samples of methyl azide ice (black line) and in the nitrogen (green line), argon, (blue line), and xenon matrix-isolated ices taken after being exposed to photolysis at 193 nm for 30 min. The insets depict magnified views of the new absorption bands, (i) HNC (ν_1), (ii) HCN (ν_1), (iii) CH_2NH (ν_2), (iv) CH_2NH (ν_3), (v) CH_2NH (ν_4), (vi) CH_2NH (ν_5), (vii) CH_2NH (ν_6), (viii) CH_2NH (ν_7), and (ix) HNC (ν_2). The band positions are compiled in Table 4.

$\pm 4 \times 10^{16}$ molecules cm^{-2} ; meanwhile, the CH_2NH column density rose continuously with increasing irradiation time to $(2.7 \pm 1.0) \times 10^{16}$ molecules cm^{-2} . On the other hand, the nitrogen (Figure 6) and argon (Figure 7) matrix-isolated ices behave differently upon electron irradiation. Here, as the methyl azide column decreased, those of the CH_2NH , HCN, and HNC increased to a maximum at about $t = 12\text{--}20$ min; thereafter, a decrease in their column densities was observed, while the CH_3N_3 column density remained constant. The column density for linear N_3 calculated from the N_2 ice sample increased to a final value of 3.8×10^{14} molecules cm^{-2} , in a similar tendency to that reported by Jamieson and Kaiser.⁵⁶

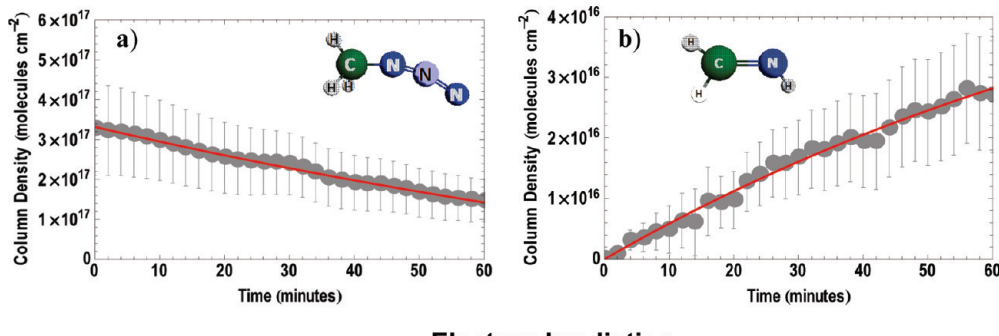
The temporal evolution of the column densities of methyl azide and the newly formed molecules during the photolysis of the pure and matrix-isolated ices are shown in Figures 5 and 8–10. Here, in the same manner as was observed in the ices under electron irradiation, the methyl azide in the ices decomposed under photolysis rapidly during the first 20 min of reaction and then remained stable. In the neat sample (Figure 5) as well as in the nitrogen and argon matrix-isolated ices (Figures 8 and 9), the column density for CH_2NH rose continuously during all of the photolysis experiments; a similar tendency was observed in the column densities of HCN and HNC. In contrast, products found from xenon matrix photodecomposition (Figure 10) showed different behavior; (i) the column density of HCN had the largest production yield of all of the new molecules during the course of this experiment, and (ii) the column density of CH_2NH exhibited a maximum at $t = 6$ min.

3. Mass Balance. To evaluate the fate of the various reactions involved, we carried out analysis of the carbon balance during the reactions based on the final abundance of product and reactant reached at long time. Table 5 shows the mass balance for electron irradiation experiments in terms of changes in (i) column densities, (ii) column densities per electron, and (iii) molecules per electron. For pure methyl azide ice, the mass balance is incomplete. This is partly due to the inability to observe HNC or HNC (only CH_2NH is seen) and clearly also due to the production of more complex polymeric products, as is evident from organic residues observed in our experiments. For experiments carried out in the matrixes, the carbon mass balance is only approximately obtained, and analysis suggests that CH_2NH , HCN, and HNC might not be the only carbon-bearing products. For example, it is well-known that CH_2NH polymerizes easily or react either with HCN or HNC (eq

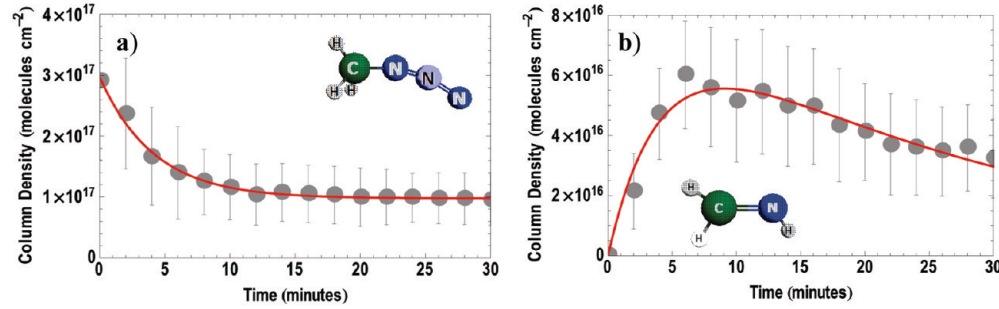
TABLE 4: New IR Absorptions Observed in the Photolyzed Samples at 10 K^a

Species	Mode	This Work			$A(\nu) \times 10^{-18}$ (cm^{-1} molec $^{-1}$)	Literature		
		pure	N_2	Ar		ref 50	ref 22	ref 39
CH_2NH	ν_2	—	3032	3035	7.96	3036		CH stretch
	ν_3	—	2919	2921	10.38	2915		CH stretch
	ν_4	1638	1637	1639	3.80	1638		C≡N stretch
	ν_5	—	1450	1452	0.96	1453		CH_2 scissors
	ν_6	—	1352	1347	7.60	1342		HCNH def
	ν_7	—	1064	1061	5.92	1055		HCNH def
HCN	ν_1	—	3286	3299	8.77	3286	11 (+4.6, -2.9)	CH stretch
	ν_2	—	741	—	12.98	746		Bend
HNC	ν_1	—	3566	3581	34.70	3565		NH stretch

^a $A(\nu)$ is the integral absorption coefficient, defined as the absorption cross section over the range of wavenumbers where the ν absorption is significant, in cm^{-1} molecule $^{-1}$.



Electron Irradiation



Photon Irradiation

Figure 5. Temporal development of the column densities during the periods of electron and photon irradiations in neat samples. The kinetic fits are also shown in red for each species according to the scheme shown in eq 11. See text for details.

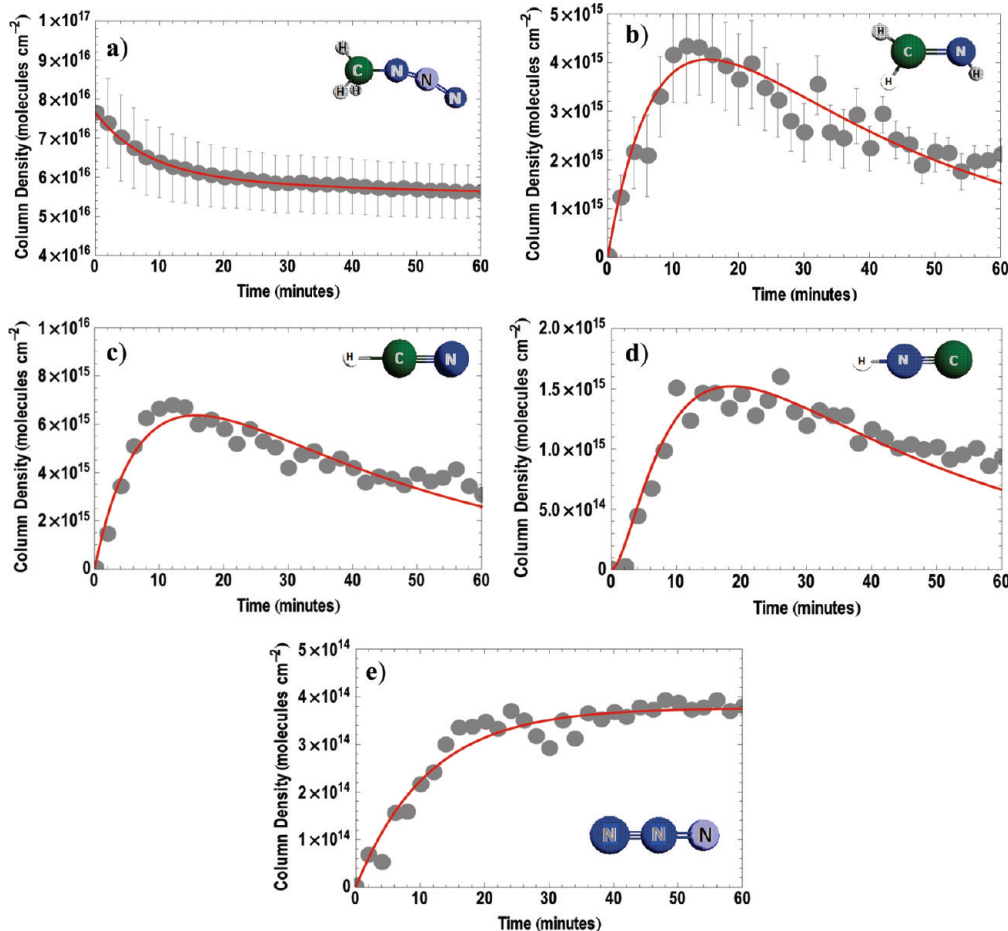


Figure 6. Temporal development of the column densities during the electron irradiation period for (a) CH_3N_3 , (b) CH_2NH , (c) HCN, (d) HNC, and (e) N_2 in a nitrogen matrix-isolated sample. The kinetic fits are also shown in red for each species according to the reaction mechanism in Figure 12a.

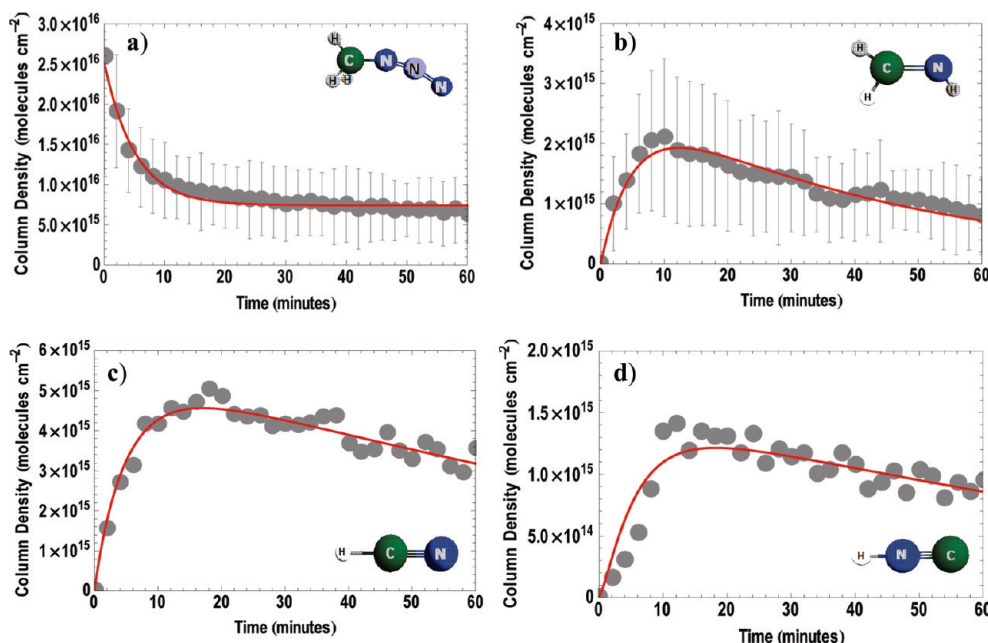


Figure 7. Temporal development of the column densities during the electron irradiation period for (a) CH_3N_3 , (b) CH_2NH , (c) HCN, and (d) HNC in an argon matrix-isolated sample. The kinetic fits are also shown in red for each species according to the reaction mechanism in Figure 12b.

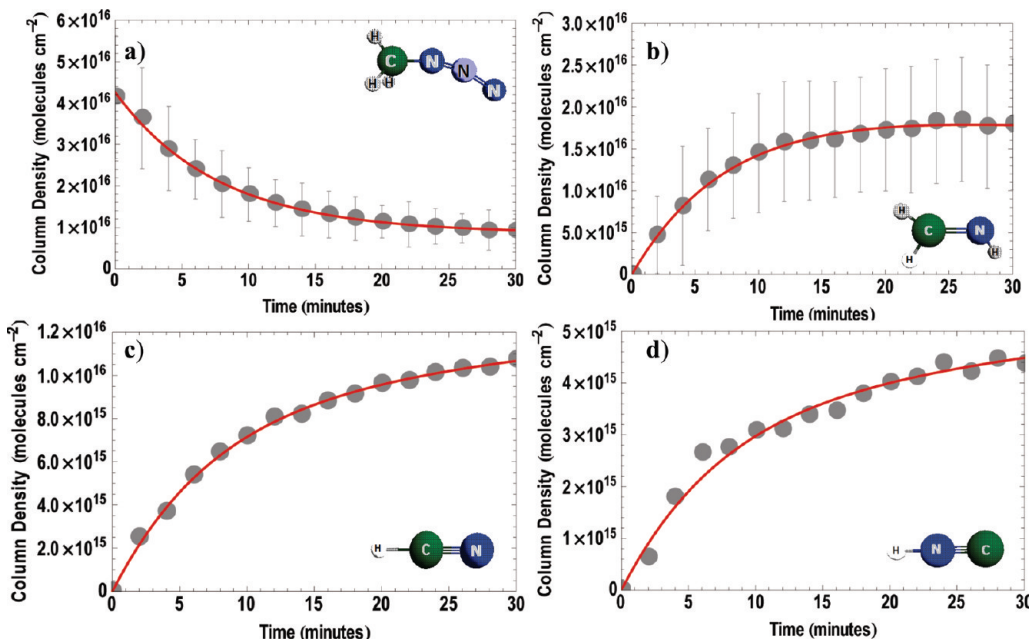


Figure 8. Temporal development of the column densities during the photolysis period for (a) CH_3N_3 , (b) CH_2NH , (c) HCN, and (d) HNC in a nitrogen matrix-isolated sample. The kinetic fits are also shown in red for each species according to the reaction mechanisms in Figure 12a.

1) at low temperatures, potentially by a concerted proton relay mechanism, to produce aminoacetonitrile.^{30,31}



Table 6 shows mass balance analysis for the 193 nm photolysis. For experiments with pure CH_3N_3 , incomplete

mass balance is seen, just as for electron irradiation, again suggesting the production of polymer, as verified experimentally. In contrast, the mass balance analysis in the matrixes all show good balance between reactants and products. To summarize, it appears that during the electron or photon irradiations for pure methyl azide samples, additional reactions are taking place, producing polymer, in contrast to the dilute matrixes. With this basic information, we now attempt analysis of the kinetics.

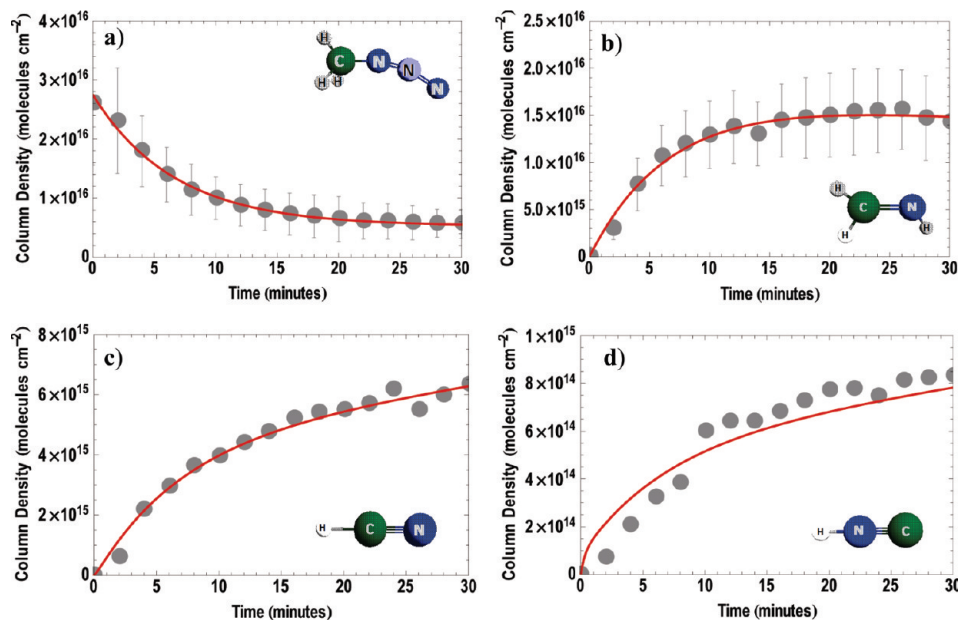


Figure 9. Temporal development of the column densities during the photolysis period for (a) CH_3N_3 , (b) CH_2NH , (c) HCN , and (d) HNC in an argon matrix-isolated sample. The kinetic fits are also shown in red for each species according to the reaction mechanism in Figure 12b.

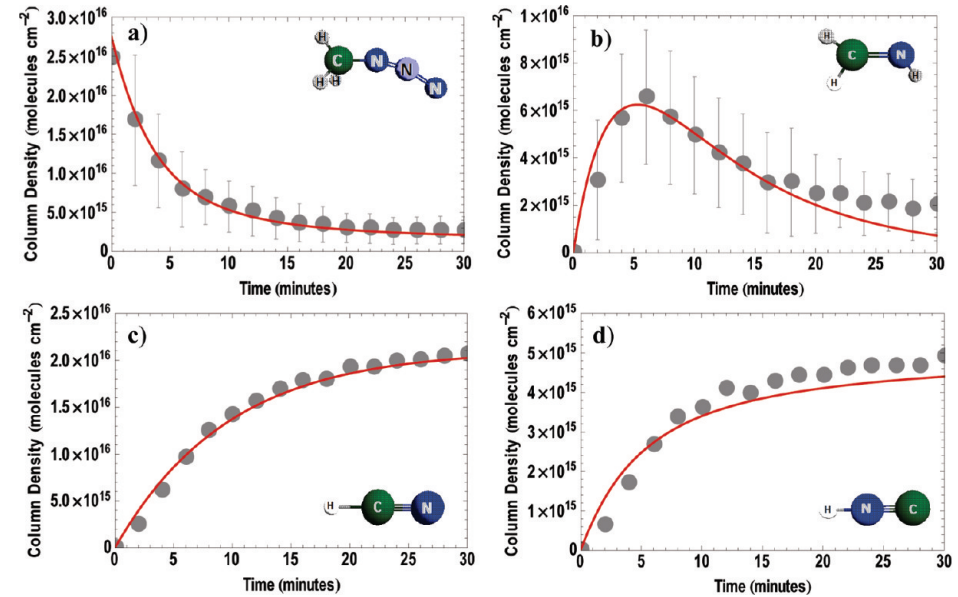


Figure 10. Temporal development of the column densities during the photolysis period for (a) CH_3N_3 , (b) CH_2NH , (c) HCN , and (d) HNC in a xenon matrix-isolated sample. The kinetic fits are also shown in red for each species according to the reaction mechanism in Figure 12c.

Discussion

1. Kinetic Models. Having identified production of CH_2NH , HCN , and HNC , resulting from irradiation of methyl azide matrix-isolated ices, and linear N_3 in the nitrogen ice exposed to electron irradiation, we turn our attention now to possible reaction pathways. As a guide, we have considered the energetic diagram shown in Figure 11, built according to the potential energy surfaces of the CH_3N_3 decomposition calculated by Nguyen et al.⁵⁸ The diagram depicts the singlet surface reaction pathways (shown as blue solid lines) in which CH_2NH , HCN , and HNC molecules are produced via molecular nitrogen followed by molecular hydrogen loss. In contrast, the triplet surface includes initial formation of ${}^3\text{CH}_3\text{N}$, which may produce CH_2N once an energy barrier of ~ 1.62 eV is overcome, followed by formation of HCN and HNC by sequential H-atom loss steps. On the basis of this information, Figure 12 shows

a general kinetic model where rate constants and solid arrows in blue indicate the pathways leading to production of HCN and HNC through the singlet surface. We complemented this model by considering relevant information reported in the literature. Thus, we included the rearrangement $\text{HCN} \rightarrow \text{HNC}$, verified already in the photolysis of HCN samples in argon ice at 4 K³⁵ and in solid Xe at 7.5 K,⁵⁴ the reverse reaction $\text{HNC} \rightarrow \text{HCN}$,⁵⁹ expected to be observed as a consequence of the relatively small isomerization energy = 30.8 kcal/mol,⁶⁰ and the potential formation of “polymer” products (shown as W, X, Y, and Z in Figure 12), as derived from the interaction of any of the molecules observed in the experiments. Final considerations were taken into account to elucidate possible reactions in our nitrogen ices, including cage recombination for the reaction $\text{CH}_2\text{NH} + \text{N}_2 \rightarrow \text{CH}_3\text{N}_3$,

TABLE 5: Balance of the Destruction of Methyl Azide (CH_3N_3) and Formation of Methanimine (CH_2NH), Hydrogen Cyanide (HCN), Hydrogen Isocyanide (HNC), and, when required, Linear N_3 after 1 h of Electron Irradiation in Pure Methyl Azide, and in Nitrogen and Argon-Isolated Methyl Azide Ices at 10 K^a

molecule	$n \times 10^{16}$ (molecules cm^{-2})	$n' \times 10^{16}$ (molecules cm^{-2})	$n'' \times 10^{16}$ (molecules cm^{-2})
CH ₃ N ₃ ice			
CH ₃ N ₃	-(18 ± 8)	-(100 ± 45)	-(300 ± 130)
CH ₂ NH	2.7 ± 0.7	15 ± 4	45 ± 12
N_2 matrix			
CH ₃ N ₃	-(2 ± 1)	-(11 ± 6)	-(33 ± 17)
CH ₂ NH	0.20 ± 0.05	1.1 ± 0.3	3.3 ± 0.9
HCN	0.35	2	6
HNC	0.1	0.6	1.8
N ₃	0.04	0.22	0.66
Ar matrix			
CH ₃ N ₃	-(2 ± 1)	-(11 ± 6)	-(34 ± 18)
CH ₂ NH	0.09 ± 0.06	0.5 ± 0.3	1.5 ± 0.1
HCN	0.35	2.0	5.9
HNC	0.1	0.6	1.8

^a Units are given in column densities (n ; molecules cm^{-2}), in molecules synthesized per electron per unit area on cm^2 (n'), and in molecules synthesized per electron (n'').

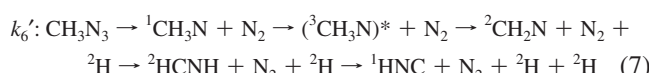
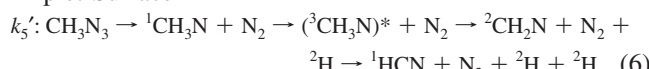
and the production of linear N_3 , as was reported to occur in nitrogen ices exposed to electron irradiation.^{55,56}

Because ${}^1\text{CH}_3\text{N}$, CH_2N , and HCN were not observed during the irradiation experiments, despite being intermediate species shown in Figure 11, we now define the rate constants for the different reaction routes as follows. Equations 6 and 7 will be explained in detail soon after.

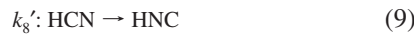
Singlet Surface



Triplet Surface



Isomerization HCN ↔ HNC



Production of Linear N₃



Using the general kinetic model in Figure 12, we proceeded initially to fit the data obtained in the photolysis of methyl azide at 193 nm. Thus, a system of four coupled differential equations was analytically solved for each scheme and used to fit the time-dependent column densities obtained from our experiments. A great variety of reaction mechanisms can be produced from this

TABLE 6: Balance of the Destruction of Methyl Azide (CH_3N_3) and Formation of Methanimine (CH_2NH), Hydrogen Cyanide (HCN), Hydrogen Isocyanide (HNC), and Hydrogen Cyanide (HCN) after 30 min of Photolysis at 193 nm in Pure Methyl Azide and in the Nitrogen, Argon, and Xenon Matrix-Isolated Ices of CH_3N_3 at 10 K^a

molecule	$n \times 10^{16}$ (molecules cm^{-2})	$n' \times 10^{-4}$ (molecules cm^{-2})	$n'' \times 10^{-4}$ (molecules cm^{-2})
CH_3N_3 ice			
CH ₃ N ₃	-(18 ± 4)	-(11.3 ± 2.5)	-(4.5 ± 1.0)
CH ₂ NH	3.0 ± 1.5	1.9 ± 1.0	0.8 ± 0.4
N_2 matrix			
CH ₃ N ₃	-(3.2 ± 1.3)	-(2.0 ± 0.8)	-(0.8 ± 0.3)
CH ₂ NH	1.8 ± 0.6	1.15 ± 0.4	0.50 ± 0.15
HCN	1.1	0.7	0.26
HNC	0.4	0.25	0.10
Ar matrix			
CH ₃ N ₃	-(2.0 ± 1.3)	-(1.2 ± 0.8)	-(0.5 ± 0.3)
CH ₂ NH	1.5 ± 0.6	0.95 ± 0.40	0.40 ± 0.15
HCN	0.65	0.4	0.16
HNC	0.08	0.05	0.02
Xe matrix			
CH ₃ N ₃	-(2.4 ± 0.6)	-(1.5 ± 0.4)	-(0.60 ± 0.15)
CH ₂ NH	0.20 ± 0.05	0.13 ± 0.03	0.05 ± 0.01
HCN	2.0	1.3	0.5
HNC	0.5	0.32	0.13

^a Units are given in column densities (n ; molecules cm^{-2}), in molecules synthesized per photon per cm^2 (n'), and in molecules synthesized per photon (n'').

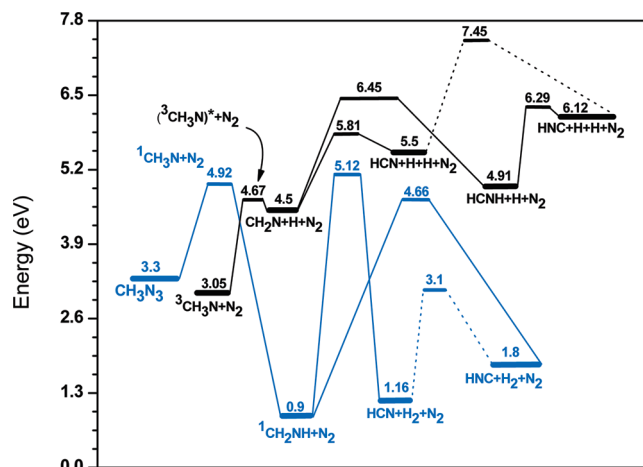


Figure 11. Energetic diagram for primary and secondary dissociation processes observed in the singlet (solid blue lines) and triplet surfaces predicted to be observed in the methyl azide dissociation. This was adapted from Nguyen et al.⁵⁸ Dotted lines correspond to the isomerization $\text{HCN} \leftrightarrow \text{HNC}$ according to Lee and Rendell.⁷⁵

kinetic model; therefore, the solved equations were manipulated to fit the data to reaction mechanisms in the singlet and triplet surfaces, or when both surfaces interact. For example, k_5' and k_6' were forced to be zero in the solved set of equations to explore if the data could best fit the production of HCN and HNC through the singlet surface.

For the 193 nm photochemistry, we found that the best fits correspond to the reaction mechanisms shown in Figure 12. These mechanisms will be explained in detail in the next section. We also used these systems of solved equations to fit the data obtained from the electron-irradiated sample in the argon ice and obtained the corresponding set of kinetic equations for those obtained in the nitrogen ice. Here, attempts to fit the data in both ices through these sets of equations failed. Attempts to fit

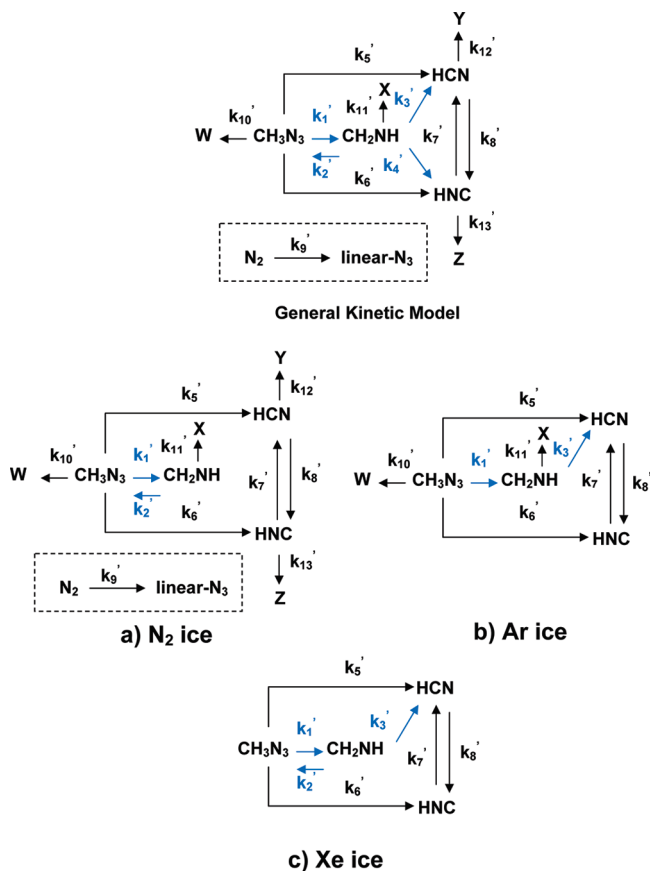


Figure 12. General kinetic model utilized to fit the temporal evolution of the methyl azide (CH_3N_3) reactant as well as the newly formed CH_2NH , HCN, HNC, and, when required, linear N_3 , as shown in Figures 6–10. The reaction mechanisms obtained in (a) nitrogen, (b) argon, and (c) xenon ice samples were proposed according to the best fits extracted from this general kinetic model for the electron and photon irradiation experiments. Dashed squares denote the production of linear N_3 observed in the nitrogen matrix-isolated ice upon electron irradiation. Rate constants k_{10}' , k_{11}' , k_{12}' , and k_{13}' were used to evaluate the probable production of other miscellaneous species (W, X, Y, and Z) originating from the interaction of CH_3N_3 , CH_2NH , HCN, and HNC, respectively. Rate constants and solid arrows in blue indicate the pathways leading to production of HCN and HNC through the singlet surface.

the data resulted in unphysical results (negative rate constants) or markedly less satisfactory fits to the data. Many physically

reasonable alternatives were tried, but none allowed us to fit the data. Only one approach appears successful and required us to assume that the integral absorption coefficient of the methyl azide changes during electron irradiation, for which there is precedence. Investigations comparable to our experimental conditions have been reported where the integrated absorption coefficients used in the Beer–Lambert relationship varied during electron irradiation as a consequence of band-broadening effects.^{61,62} If that were true in our case, the differential equations would have to be modified.

The differential equations obtained from the general kinetic model in Figure 12 are shown in the Appendix for the case where they have been modified to describe the time-dependent absorption strength; an absorption correction factor, a_0 , was introduced. Once analytically solved, the equations were manipulated again to fit the data according to the possible reaction mechanisms in the singlet and triplet surfaces. For both types of irradiation experiments, the best fits to our data occurred according to the reaction mechanisms shown in Figure 12a–c, similarly to our initial fits where the absorption correction factor was not considered. Our results suggest that the dissociation of methyl azide is influenced strongly by the matrixes in which the reactions took place.

2. Reaction Mechanisms. The rate constants extracted from the best fits from the general kinetic model in all of our matrix samples are present in Table 7. The best fits are shown in solid red lines over the temporal evolutions of the column densities of the individual species in the nitrogen (Figures 6 and 8), argon (Figures 7 and 9), and xenon (Figure 10).

In the nitrogen ices, the most reasonable explanation for the processes induced by photon or electron irradiation is a recombination to CH_3N_3 , as indicated in Figure 12a, which also implies production of HCN and HNC through a portion of the triplet surface. We never were able to fit our data under reaction mechanisms involving secondary decomposition of CH_2NH to HCN and HNC, as the singlet potential surface dictates. If we assume that recombination k_2' is important, then the production of HCN and HNC through secondary dissociations is minimized, explaining our less satisfactory fit to data using reaction mechanisms in the singlet surface. When we best fit the data of the CH_3N_3 decomposition in the nitrogen ice upon electron irradiation, we found that the rate constant k_9' is $(1.45 \pm 0.20) \times 10^{-3} \text{ s}^{-1}$. This value is in close agreement to that reported by Jamieson and Kaiser⁵⁶ $((1.2 \pm 0.1) \times 10^{-3} \text{ s}^{-1})$, which was obtained in the radiolysis of nitrogen ice. This result may suggest

TABLE 7: Compilation of Rate Constants as Extracted from the Kinetic Fits of the Column Densities of Methyl Azide and Its Products According to the Selected Reaction Mechanisms That Best Fit the Data in Figures 5–10

	Reaction Rate ($\times 10^{-3} \text{ s}^{-1}$)					
	electron irradiation			photon irradiation		
	pure	N_2	Ar	pure	N_2	Ar
k_1'	0.017 ± 0.005	0.6 ± 0.2	0.5 ± 0.2	1.6 ± 0.4	1.3 ± 0.4	1.9 ± 0.4
k_2'		0.9 ± 0.3			0.2 ± 0.1	
k_3'			0.4 ± 0.1			0.10 ± 0.03
k_4'						
k_5'		1.1 ± 0.3	1.1 ± 0.3		0.80 ± 0.15	0.35 ± 0.10
k_6'		0.02 ± 0.01	0.12 ± 0.03		0.010 ± 0.005	0.25 ± 0.10
k_7'		3.0 ± 1.3	10 ± 4		75 ± 20	48 ± 8
k_8'		1.7 ± 0.5	2.7 ± 0.8		32 ± 10	6 ± 2
k_9'		1.45 ± 0.20				
k_{10}'	0.09	0.01	1.2	2.4	0.001	0.08
k_{11}'	0.045	0.01	0.3	0.02	0.015	0.16
k_{12}'		0.01				
k_{13}'		3.9				

that the production of linear N₃ is a reaction hardly influenced by the decomposition of CH₃N₃ when it occurs in the nitrogen ice under electron irradiation and most probably is simply a secondary matrix effect.

In the argon ices, the best fit to our data suggests that the methyl azide decomposition occurs through an irreversible reaction mechanism on the singlet surface and production of HCN and HNC on the triplet one, as is indicated in Figure 12b. Once CH₂NH is produced, a secondary dissociation to HCN followed by a rapid isomerization HCN → HNC is most probable. According to our fits, production of HNC from CH₂NH was quite ambiguous. A simple inspection of our energy diagram (Figure 11) suggests that the large energy (4.22 eV) to this reaction supports this finding, in contrast to the small-energy isomerization of HCN → HNC. Therefore, if the reaction CH₂NH → HNC+H₂ occurs, it must be quite limited.

The best fits of photolysis of methyl azide in xenon ice are presented in Figure 10. Unlike the previous dissociations, the mechanism of methyl azide in xenon ice (Figure 12c) suggests that CH₂NH recombines to produce CH₃N₃ and simultaneously decomposes through a secondary dissociation to produce HCN. Also, our results suggest that CH₃N₃ decomposes to produce triplet species, leading to the formation of HCN and HNC. We speculate that in xenon ice, the diffusion of the molecular N₂ produced from the degradation of CH₃N₃ could have been restricted and located in a close neighborhood to the nascent CH₂NH. This suggestion is reasonable because we never observed bands of other products produced potentially from CH₂NH, implying that some of its molecules could have reacted immediately with the available molecular nitrogen forming CH₃N₃.

For analysis of pure ices, a different kinetic analysis was required. Recall that during the electron and photon irradiations of pure methyl azide, the only newly formed molecule observed was CH₂NH; however, the formation of methanimine alone could not account quantitatively for the rapid decay of the column densities of the CH₃N₃ reactants observed in both irradiations (Figure 5). Because neither HCN, HNC, nor any other molecular carriers were detectable in the IR spectra, we introduced a separate kinetic scheme to fit the experimental profiles of the methyl azide and CH₂NH species, as shown in eq 11.



where W and X represent some undefined species or polymer produced upon irradiation. The differential models are also included in the Appendix (eqs 14 and 15), and the resulting fits are shown in Figure 5 (as red solid lines) and in Table 7. This mechanism was capable of fitting the data for both photon and electron irradiation. Our results suggest that the reaction CH₃N₃ → CH₂NH is present, and that generic polymer is produced directly from both species.

A final comment on the role of other products produced in the nitrogen and argon ices was also carried out. Broad bands in the range of 2900–3200 cm⁻¹ might suggest that species such as azomethane (CH₃NNCH₃), N-methyl methanimine (CH₂NHCH₃), and trimers of CH₂NH and HCN could also have been produced. Table 7 shows that the rate constants k₁₀'–k₁₃', considered to evaluate production of these miscellaneous species, agree with the observation of such broad bands.

3. Is the Triplet Pathway a Reliable Route Leading to HCN and HNC? CH₃N₃ is singlet in its ground state; therefore, the most probable dissociation process should occur on the

singlet potential surface, as was observed through the production of CH₂NH. However, we were unable to successfully fit our data by considering only reaction mechanisms in which HCN and HNC are produced by secondary dissociation of CH₂NH. Therefore, other possible reactions including formation of products via the triplet surface were considered.

Currie and Darwent⁶³ concluded that methyl nitrene (CH₃N) is involved in an important secondary reaction in the gas-phase photolysis of methyl azide, leading to reaction 12



More recently, Larson et al., through collision-free VUV photoionization-based photofragmentation translational spectroscopy (PTS) studies, verified that ¹CH₃N and N₂ are the primary products in the photolysis of methyl azide at 193⁶⁴ and 248⁶⁵ nm. In the matrix environment, rapid rearrangement of ¹CH₃N to CH₂NH might be dominant due to the rapid removal of excess energy from the free radical species through collisions with the matrix. Unlike gas-phase photolysis, in our matrix experiments, ¹CH₃N might react with CH₃N₃, allowing production of azomethane, as Currie and Darwent⁶³ suggested. This might mean that some of the bands identified as “miscellaneous species”, in fact correspond to azomethane. Alternatively, part of ¹CH₃N might undergo intersystem crossing (ISC) to the triplet surface; see Figure 11. Once on the triplet potential surface, the barrier to form HCN is ~1.30 eV from CH₂N, and there is a maximum barrier of ~1.95 eV to HNC, in comparison to 4.22 and 3.76 eV, if CH₂NH decomposes to the same products. This suggests that the former processes might be competitive with the latter under some circumstances. To test the validity of this mechanistic idea, we re-examined our results from the 193 nm photolysis of CH₃N₃ in xenon ice. Here, the rate constants obtained by its presence are enhanced (see Table 7), an effect that is typically known as the heavy-atom effect.⁶⁶ This suggests that the ISC ¹CH₃N → (³CH₃N)*, as depicted in Figure 13, might be possible. If ¹CH₃N were responsible for producing other species like CH₃N=NCH₃, such production would be expected to decrease in the xenon ice as a consequence of a faster conversion of ¹CH₃N to the triplet surface. This is consistent with our observations. In light of our current results, ISC is the most reasonable explanation for the production of a portion of the HCN and HNC. Further work would help to settle this question.

The photochemistry of methyl azide, studied previously in our group using the PTS technique at 193 nm,⁶⁴ also agrees with these assessments. In this work, we found that the production of HCN through sequential loss of two H-atoms is dominant over the formation of HCN or HNC by H₂ elimination; in other words, the secondary dissociations of HCN and HNC from CH₂NH must be minor channels. If one also considers that, in works comparable to our experimental conditions, the isomerization HCN → HNC has been demonstrated already,^{35,54} one can assume that HCN produced from the dominant channel is a major source for HNC molecules. On the other hand, we have indicated already that another source of HNC molecules is also through the sequential loss of two H-atoms from CH₂N. This pathway requires that CH₂N isomerizes first to HCNH (eq 7) and overcomes two energy barriers (Figure 11), which suggests that this process potentially might be less competitive with the isomerization HCN → HNC. Consequently, from the rate constants used to evaluate pathways leading to HNC (k₄', k₆', and k₈'), that for the reaction HCN → HNC (k₈') should be noted as the largest one. An inspection of Table 7 reveals that this condition is satisfied by our best fits in all of the samples.

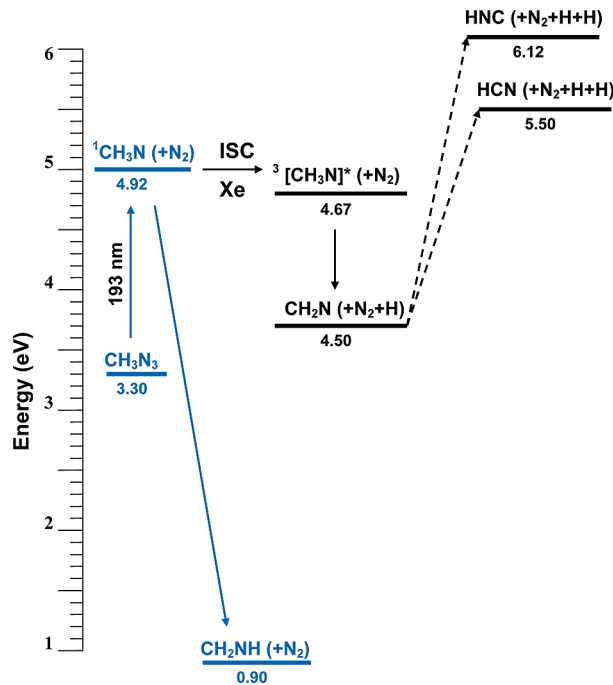


Figure 13. Schematic picture of the photodissociation of methyl azide following the 193 nm photon irradiation at low temperature in the xenon sample. Broken bars represent subsequent dissociations yielding HCN and HNC according to Figure 11.

A more detailed analysis on the rate constant k_8' is depicted as follow. Considering the fate of HCN and HNC, we inspected the temporal behavior of the ratio of $[\text{HCN}]/[\text{HNC}]$. This ratio is shown for different matrixes relevant to electron irradiation (Figure 14a) and photolysis (Figure 14b). After an initial induction time, HCN and HNC concentrations appear to approach an equilibrium (or steady-state relationship) with one another. Therefore, the ratio $[\text{HCN}]/[\text{HNC}]$ will tend toward $K_{\text{eq}} \approx k_7'/k_8'$. For the electron irradiation (Figure 14a), the ratios $[\text{HCN}]/[\text{HNC}]$ in the N_2 and Ar matrixes tend toward ~ 3.5 , and for the photolysis experiments (Figure 14b), they tend to 2.2, 7.2, and 4.4 for the N_2 , Ar, and Xe matrixes. The best fits indicate that the isomerization $\text{HCN} \leftrightarrow \text{HNC}$ occurs, and an analysis comparing ratios of k_7'/k_8' for each matrix leads to similar ratios (within the errors of the rate constants) and tends to support the statement that the HCN and HNC, once formed, approach equilibrium with one another.

4. Energy Balance Calculations. As a common sense check of the interpretation of the experiment, we consider energy balance. We present in this section simple calculations for the neat methyl azide samples. We may estimate the amount of energy deposited in the matrix by the electrons and photons and compare this to the amount of energy needed to degrade the number of methyl azide molecules seen destroyed in the kinetics experiments.

We first consider the electron irradiation experiments. As mentioned previously, a typical electron flux in our experiments was 5.9×10^{14} electrons cm^{-2} , giving an electron dose of 1.8×10^{15} electrons. Each electron carries 5 keV of energy as it enters the matrix. We used the Monte Carlo Simulation of Electron Trajectory in Solids (CASINO) program⁶⁷ to characterize the average energy deposited by the electrons into the matrix. Here, the electron bombardment was simulated by 200 000 trajectories through a homogeneous ice layer of CH_3N_3 with a thickness of 360 nm, similar to the actual conditions of our experiment. The CASINO simulations led to the conclusion that

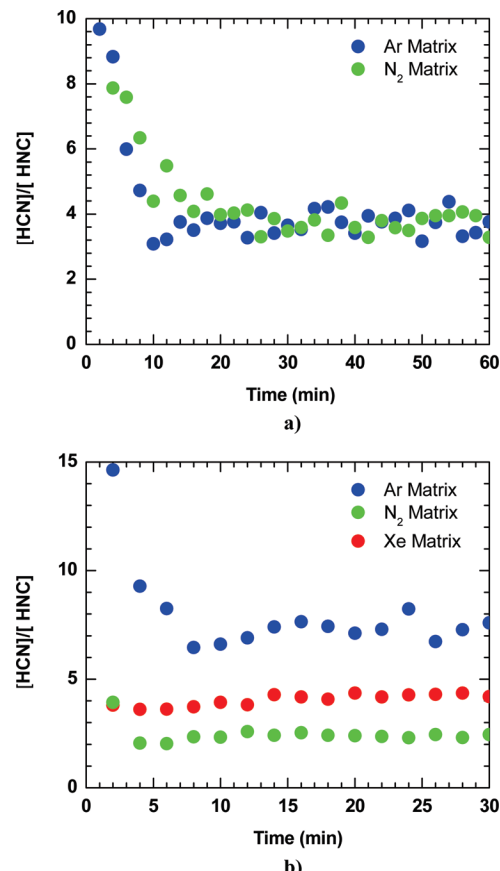


Figure 14. Temporal evolutions of the column densities of HCN/HNC in the matrix-isolated ices exposed to (a) electron and (b) photon irradiations. Curves shown in green, blue, and red correspond to the ratios of $[\text{HCN}]/[\text{HNC}]$ that were obtained from the nitrogen, argon, and xenon solids.

$\sim 26\%$ of the energy of each 5 keV electron is transferred to the matrix. Combining this with the electron dose, we derived that the matrix absorbed was $\sim 2.4 \times 10^{18}$ eV ($\sim 5.54 \times 10^{19}$ kJ mol^{-1}) from the electron dose.

In order to dissociate methyl azide, we assume that it is necessary to at least excite the molecule with enough internal energy to access the singlet methylnitrene (${}^1\text{CH}_3\text{N} + \text{N}_2$). According to theoretical calculations of the gas-phase molecule (see also the discussion and references surrounding Figure 11), we assume the following energetics for this reaction



By analyzing the kinetic decays that are followed by IR absorption, we may also estimate that during the electron dose, we destroy 5.4×10^{17} CH_3N_3 molecules. The energy required to promote this number of methyl azide molecules at least to an energy level of 1.63 eV is then 8.8×10^{17} eV, which is about 37% of the total energy deposited in the matrix by the electron dose. Hence, we see that there is certainly enough energy in the electron doses of this work to account for the observed amount of dissociation.

For photolysis, we assume the UV absorption cross section of methyl azide to be $\sigma = 10^{-19} \text{ cm}^2$. The reader shall keep in mind that the absorption cross section can change from the gas phase to the solid state.⁶⁸ The column density of the methyl azide ice was derived to be 3×10^{17} molecules cm^{-2} , meaning that only 3% of the photon dose was absorbed. A typical photon

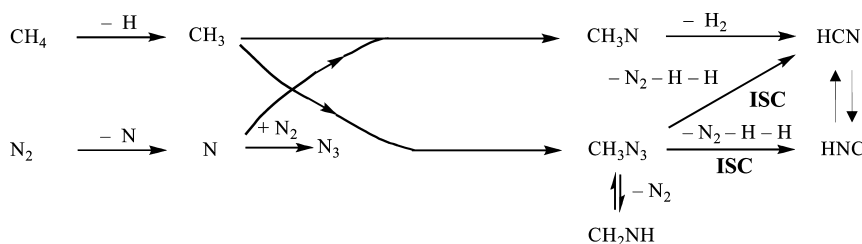


Figure 15. Compilation of elementary processes starting from methane (CH_4) and molecular nitrogen (N_2) which may trigger a carbon–nitrogen-based chemistry, such as that on Titan’s aerosol particles, via interaction with ionizing radiation if the reactions occurred in a nitrogen environment. See text for further details.

dose consisted of 1.7×10^{20} photons, 3% of which is 5×10^{18} photons. Each photon carries 6.4 eV, meaning that the photolysis deposits $\sim 3 \times 10^{19}$ eV. In the photolysis experiments, we destroyed 6.4×10^{16} methyl azide molecules, as found by the change in IR absorption. Again, assuming that energizing the molecules with at least 1.63 eV is needed to initiate dissociation, we arrive at the result that 10.4×10^{16} eV is needed to achieve the dissociation observed by IR absorption kinetics, which is $\sim 0.35\%$ of the energy deposited in the matrix by the photolysis.

5. Astrophysical Implications. Our photolysis and electron irradiation exposures of methyl azide provided insight into processes likely to occur in solid CH_4-N_2 aerosol particles in Titan’s troposphere, as well as on rich CH_4-N_2 ice surfaces such as those on Pluto and Triton and on the C/1995 O1 (Hale–Bopp) cometary ices once exposed to ambient ionizing radiation. For example, if methyl azide were synthesized at about the lower limit of the CH_4 ice cloud in Titan’s troposphere,^{10,11} at ~ 19 km above Titan’s surface, such a process could occur through the independent production of methyl and azide radicals. At this altitude, because nitrogen molecules are estimated to be contained up to 14% in the CH_4 ice particles,¹² it is possible that they can undergo unimolecular decomposition by ionizing radiation ($\sim 4.5 \times 10^9$ eV cm^{-2} s^{-1}),¹⁶ thus generating two nitrogen atoms.⁵⁶ These nitrogen atoms can have kinetic energies of a few eV; thus, they can overcome barriers to addition to a second molecular nitrogen molecule yielding the linear N_3 radical.⁵⁶ Independent groups^{55,56} have reported the production of linear N_3 when pure N_2 ices are exposed to energetic electrons, and its formation has been known as a signature of radiolysis at low temperatures. Likewise, the surrounding CH_4 ice can provide a great variety of products when exposed to electron irradiation, but the initial degradation product, the CH_3 radical, is proven to form because it has been identified completely under similar experimental conditions.⁶⁹ If these radicals are in close proximity, they can recombine to form methyl azide. Jamieson et al.¹⁷ studied an ice mixture of CH_4 and N_2 , and identified a band attributable to the strongest absorption of CH_3N_3 or HN_3 . Even when this experiment reported no distinction between such species, CH_3N_3 was likely a product; therefore, formation of methyl azide is reasonable in Titan’s troposphere, or anywhere where ice mixtures of N_2 and CH_4 are irradiated energetically. Alternatively, nitrogen atoms could react with the methyl radical, yielding CH_3N ; the latter could undergo unimolecular decomposition to form HCN.¹⁷ These reaction pathways together with those extracted from the N_2 matrixes presented in this study are compiled in Figure 15 and allow us to hypothesize about a possible kinetic scheme of CH_3N_3 in Titan.

Some points are important to note for the role of CH_2NH in astrochemistry. In cometary ices²¹ and in interstellar clouds,^{18–20} the presence of HNC has been long regarded as a hallmark in the formation and evolution of comets, and monitoring the ratio

HNC/HCN in the coma when the comet approaches the Sun has become a valuable tool to gain insight into them. Some works^{28,70} have hypothesized that the increase of such a ratio can be attributed to the photodissociation of the CH_2NH constituent in the nucleus of comets to HNC, as can occur when the comet Hale–Bopp (abundance $< 0.032\%$)²¹ is exposed to the UV solar energy, and once this solid-state reaction takes place, HNC is released to the coma by sublimation. We speculate that this possibility is remote; our irradiation experiments indicate that CH_2NH would dissociate primarily to HCN and then isomerize to HNC or polymerize. In a more real context, whether the irradiation of CH_2NH in an H_2O matrix would be carried out, as probably can occur on the comet’s nucleus, the abundance of protons in water ice might produce aminoacetonitrile, as several theoretical works have proposed.^{30,31}

A similar scheme on the dissociation from CH_2NH to HNC has been proposed to occur on the surfaces of Triton and Pluto, where nitrogen-rich ices containing small amounts of methane^{71,72} are exposed to energetic radiation from the Sun (UV flux and solar wind) and galactic cosmic rays (GCRs), the latter being radiation that dominates at both surfaces.^{22,73,74} The work of Moore and Hudson²² verified the formation of these molecules via proton irradiations of $\text{N}_2/\text{CH}_3\text{NH}_2$ ice (100:1) and speculated that CH_2NH on these ice surfaces is the intermediate compound to HNC. The results of our nitrogen solid sample suggest that the production of HCN or HNC from CH_2NH , if any, is limited, as Moore and Hudson concluded in the case for HCN.

Conclusions

Five important results emerge from the present study on the methyl azide decomposition induced by photons or electrons at low temperatures:

1. In the neat samples, the fragmentation pathway of CH_3N_3 to CH_2NH plus N_2 was identified. HCN and HNC could have been formed from CH_3N_3 and CH_2NH .
2. In the nitrogen ices, once CH_3N_3 is decomposed, cage effects favor the recombination of CH_2NH with neighboring N_2 to recycle CH_3N_3 . No evidence was found for the formation of HCN and HNC from a secondary decomposition of CH_2NH .
3. In the argon ices, the most probable route after CH_3N_3 decomposition is an irreversible production of CH_2NH . Then, a secondary decomposition of the latter produces HCN, followed by a rapid isomerization to HNC. Pathways leading to HCN and HNC through triplet species are also probable to occur.
4. In the xenon ice, when CH_2NH molecules are formed, one portion must recombine to produce CH_3N_3 , and another one dissociates to HCN and then rearranges to HNC. As in the nitrogen and argon samples, portions of HCN and HNC molecules could also be produced via triplet species. Considering that the heavy atom effect was observed in the xenon ice

experiment, we proposed that such a portion of the triplet surface is an ISC at the energy levels of ¹CH₃N → ³(CH₃N)*.

5. In all of the matrix ices, the final fate of HCN and HNC is an isomerization HCN ↔ HNC.

Acknowledgment. This project was supported by the Chemistry Division of the U.S. National Science Foundation within the Collaborative Research in Chemistry Program (NSF-CRC CHE-0627854). A.Q.H. is indebted to the National Council for Science and Technology (CONACYT-Mexico) and the University of California Institute for Mexico and the United States (UC-MEXUS) for the continuing financial support. A.Q.H. further thanks the UH NASA Astrobiology Institute for support of his accommodations at the University of Hawaii at Manoa. C.J.B. and A.Q.H. thank the National Aeronautics Space Administration (NASA-Astrobiology Institute under Cooperative Agreement no. NNA09DA77A issued through the Office of Space Science). We are also grateful to Dr. Gu (Department of Chemistry, University of Hawaii at Manoa) for his technical assistance.

Appendix

The following differential models were used for the kinetic analysis in this work. Once the solved equations were obtained, they were used to best fit the temporal evolutions of the column densities of the observed species shown in Figures 5–10. Equation 20 was included in the differential model only when the column density of the linear N₃ radical was obtained from the nitrogen ice sample exposed to electron irradiation. The differential equations were organized in a matrix and solved using the inverse Laplace method.⁷⁶ All of the rate constants were obtained in units of s⁻¹.

Model for CH₃N₃ ice

$$\frac{d([CH_3N_3] - a0)}{dt} = -(k_1' + k_{10}')[CH_3N_3] - a0 + k_2'[CH_2NH] \quad (14)$$

$$\frac{d[CH_2NH]}{dt} = k_1'([CH_3N_3] - a0) - (k_2' + k_{11}')[CH_2NH] \quad (15)$$

Model for CH₃N₃ matrix-isolated ices exposed to photon and electron irradiations

$$\frac{d([CH_3N_3] - a0)}{dt} = -(k_1' + k_5' + k_6' + k_{10}')[CH_3N_3] - a0 + k_2'[CH_2NH] \quad (16)$$

$$\frac{d[CH_2NH]}{dt} = k_1'([CH_3N_3] - a0) - (k_2' + k_3' + k_4' + k_{11}')[CH_2NH] \quad (17)$$

$$\frac{d[HCN]}{dt} = k_5'([CH_3N_3] - a0) - (k_8' + k_{12}')[HCN] + k_7'[CH_2NH] + k_7'[HNC] \quad (18)$$

$$\frac{d[HNC]}{dt} = k_6'([CH_3N_3] - a0) - (k_7' + k_{13}')[HNC] + k_4'[CH_2NH] + k_8'[HCN] \quad (19)$$

$$\frac{d[N_3]}{dt} = k_9'[N_2] \quad (20)$$

References and Notes

- (1) Raulin, F.; Khelifi, M.; Dang-Nhu, M.; Gautier, D. *Adv. Space Res.* **1992**, *12*, 181.
- (2) Bruston, P.; Khelifi, M.; Benilan, Y.; Raulin, F. *J. Geophys. Res., Planets* **1994**, *99*, 19047.
- (3) Raulin, F.; Bruston, P.; Paillous, P.; Sternberg, R. *Life Sci. Space Res.* **25**(4) **1994**, *15*, 321.
- (4) Thompson, W. R.; Henry, T. J.; Schwartz, J. M.; Khare, B. N.; Sagan, C. *Icarus* **1991**, *90*, 57.
- (5) Khelifi, M.; Paillous, P.; Bruston, P.; Raulin, F.; Guillemin, J. C. *Icarus* **1996**, *124*, 318.
- (6) Niemann, H. B.; Atreya, S. K.; Bauer, S. J.; Carignan, G. R.; Demick, J. E.; Frost, R. L.; Gautier, D.; Haberman, J. A.; Harpold, D. N.; Hunten, D. M.; Israel, G.; Lunine, J. I.; Kasprzak, W. T.; Owen, T. C.; Paulkovich, M.; Raulin, F.; Raaen, E.; Way, S. H. *Nature* **2005**, *438*, 779.
- (7) Fulchignoni, M.; Ferri, F.; Angrilli, F.; Ball, A. J.; Bar-Nun, A.; Barucci, M. A.; Bettanini, C.; Bianchini, G.; Borucki, W.; Colombatti, G.; Coradini, M.; Coustenis, A.; Debei, S.; Falkner, P.; Fanti, G.; Flamini, E.; Gaborit, V.; Grard, R.; Hamelin, M.; Harri, A. M.; Hathi, B.; Jernej, I.; Leese, M. R.; Lehto, A.; Stoppato, P. F. L.; Lopez-Moreno, J. J.; Makinen, T.; McDonnell, J. A. M.; McKay, C. P.; Molina-Cuberos, G.; Neubauer, F. M.; Pirronello, V.; Rodrigo, R.; Saggin, B.; Schwingenschuh, K.; Seiff, A.; Simoes, F.; Svedhem, H.; Tokano, T.; Towne, M. C.; Trautner, R.; Withers, P.; Zarnecki, J. C. *Nature* **2005**, *438*, 785.
- (8) Barth, E. L.; Toon, O. B. *Icarus* **2006**, *182*, 230.
- (9) Graves, S. D. B.; McKay, C. P.; Griffith, C. A.; Ferri, F.; Fulchignoni, M. *Planet. Space Sci.* **2008**, *56*, 346.
- (10) Tokano, T.; McKay, C. P.; Neubauer, F. M.; Atreya, S. K.; Ferri, F.; Fulchignoni, M.; Niemann, H. B. *Nature* **2006**, *442*, 432.
- (11) Atreya, S. K.; Adams, E. Y.; Niemann, H. B.; Demick-Montelara, J. E.; Owen, T. C.; Fulchignoni, M.; Ferri, F.; Wilson, E. H. *Planet. Space Sci.* **2006**, *54*, 1177.
- (12) Wang, C. C.; Atreya, S. K.; Signorell, R. *Icarus* **2010**, *206*, 787.
- (13) Flasar, F. M.; Achterberg, R. K.; Conrath, B. J.; Giersch, P. J.; Kunde, V. G.; Nixon, C. A.; Bjoraker, G. L.; Jennings, D. E.; Romani, P. N.; Simon-Miller, A. A.; Bezard, B.; Coustenis, A.; Irwin, P. G. J.; Teanby, N. A.; Brasunas, J.; Pearl, J. C.; Segura, M. E.; Carlson, R. C.; Mamoutkine, A.; Schindler, P. J.; Barucci, A.; Courtin, R.; Fouchet, T.; Gautier, D.; Lellouch, E.; Marten, A.; Prange, R.; Vinatier, S.; Strobel, D. F.; Calcutt, S. B.; Read, P. L.; Taylor, F. W.; Bowles, N.; Samuelson, R. E.; Orton, G. S.; Spilker, L. J.; Owen, T. C.; Spencer, J. R.; Showalter, M. R.; Ferrari, C.; Abbas, M. M.; Raulin, F.; Edgington, S.; Ade, P.; Wishnow, E. H. *Science* **2005**, *308*, 975.
- (14) Sagan, C.; Thompson, W. R. *Icarus* **1984**, *59*, 133.
- (15) Borucki, W. J.; Levin, Z.; Whitten, R. C.; Keesee, R. G.; Capone, L. A.; Summers, A. L.; Toon, O. B.; Dubach, J. *Icarus* **1987**, *72*, 604.
- (16) Molina-Cuberos, G. J.; Lopez-Moreno, J. J.; Rodrigo, R.; Lara, L. M.; O'Brien, K. *Planet. Space Sci.* **1999**, *47*, 1347.
- (17) Jamieson, C. S.; Chang, A. H. H.; Kaiser, R. I. *Adv. Space Res.* **2009**, *43*, 1446.
- (18) Kaifu, N.; Morimoto, M.; Nagane, K.; Akabane, K.; Iguchi, T.; Takagi, K. *Astrophys. J.* **1974**, *L135*.
- (19) Godfrey, P. D.; Brown, R. D.; Robinson, B. J.; Sinclair, M. W. *Astrophys. Lett. Commun.* **1973**, *13*, 119.
- (20) Dickens, J. E.; Irvine, W. M.; DeVries, C. H.; Ohishi, M. *Astrophys. J.* **1997**, *479*, 307.
- (21) Crovisier, J.; Bockele-Morvan, D.; Colom, P.; Biver, N.; Despois, D.; Lis, D. C. *Astron. Astrophys.* **2004**, *418*, 1141.
- (22) Moore, M. H.; Hudson, R. L. *Icarus* **2003**, *161*, 486.
- (23) Vuitton, V.; Yelle, R. V.; Anicich, V. G. *Astrophys. J.* **2006**, *647*, L175.
- (24) Snyder, L. E.; Buhl, D. *Astrophys. J.* **1971**, *163*, L47.
- (25) Boonman, A. M. S.; Stark, R.; van der Tak, F. F. S.; van Dishoeck, E. F.; van der Wal, P. B.; Schafer, F.; de Lange, G.; Laauwen, W. M. *Astrophys. J.* **2001**, *553*, L63.
- (26) Bockeleemorvan, D.; Padman, R.; Davies, J. K.; Crovisier, J. *Planet. Space Sci.* **1994**, *42*, 655.
- (27) Magee-Sauer, K.; Mumma, M. J.; DiSanti, M. A.; Dello Russo, N.; Rettig, T. W. *Icarus* **1999**, *142*, 498.
- (28) Irvine, W. M.; Dickens, J. E.; Lovell, A. J.; Schloerb, F. P.; Senay, M.; Bergin, E. A.; Jewitt, D.; Matthews, H. E. *Faraday Discuss.* **1998**, *475*.
- (29) Biver, N.; Bockele-Morvan, D.; Crovisier, J.; Colom, P.; Henry, F.; Moreno, R.; Paubert, G.; Despois, D.; Lis, D. C. *Earth, Moon, Planets* **2002**, *90*, 323.
- (30) Bernstein, M. P.; Bauschlicher, C. W., Jr.; Sandford, S., A., *Adv. Space Res.* **2004**, *33*, 40.
- (31) Koch, D. M.; Toubin, C.; Peslherbe, G. H.; Hynes, J. T. *J. Phys. Chem.* **2008**, *112*, 2972.
- (32) Milligan, D. E. *J. Chem. Phys.* **1961**, *35*, 1491.
- (33) Jacox, M. E.; Milligan, D. E. *J. Mol. Spectrosc.* **1975**, *56*, 333.
- (34) Milligan, D. E.; Jacox, M. E. *J. Chem. Phys.* **1963**, *39*, 712.
- (35) Milligan, D. E.; Jacox, M. E. *J. Chem. Phys.* **1967**, *47*, 278.
- (36) Ferrante, R. F. *J. Chem. Phys.* **1987**, *86*, 25.
- (37) Barash, L.; Wassermann, E.; Yager, W. A. *J. Am. Chem. Soc.* **1967**, *89*, 3931.

- (38) Carrick, P. G.; Engelking, P. C. *J. Chem. Phys.* **1984**, *81*, 1661.
- (39) Hassner, A.; Stern, M.; Gottlieb, H. E.; Frolow, F. *J. Org. Chem.* **1990**, *55*, 2304.
- (40) Bennett, C. J.; Jamieson, C.; Mebel, A. M.; Kaiser, R. I. *Phys. Chem. Chem. Phys.* **2004**, *6*, 735.
- (41) Bennett, C. J.; Osamura, Y.; Lebar, M. D.; Kaiser, R. I. *Astrophys. J.* **2005**, *634*, 698.
- (42) Lee, C. T.; Yang, W. T.; Parr, R. G. *Phys. Rev. B* **1988**, *37*, 785.
- (43) Becke, A. D. *J. Chem. Phys.* **1993**, *98*, 5648.
- (44) Schmidt, M. W.; Baldridge, K. K.; Boatz, J. A.; Elbert, S. T.; Gordon, M. S.; Jensen, J. H.; Koseki, S.; Matsunaga, N.; Nguyen, K. A.; Su, S. J.; Windus, T. L.; Dupuis, M.; Montgomery, J. A. *J. Comput. Chem.* **1993**, *14*, 1347.
- (45) Douglas, D. T.; Durig, M. S.; Durig, J. R. *Spectrochim. Acta, Part A* **2005**, *61*, 1287.
- (46) Basiuk, V. A.; Navarro-Gonzalez, R.; Benilan, Y.; Raulin, F. *Spectrochim. Acta, Part A* **2000**, *56*, 1157.
- (47) Wang, Z. Z. *J. Mol. Struct.: THEOCHEM* **1998**, *434*, 1.
- (48) Mantica, E.; Zerbi, G. *Gazz. Chim. Ital.* **1960**, *90*, 53.
- (49) Miller, F. A.; Bassi, D. *Spectrochim. Acta* **1963**, *19*, 565.
- (50) Hamada, Y.; Hashiguchi, K.; Tsuboi, M.; Koga, Y.; Kondo, S. *J. Mol. Spectrosc.* **1984**, *105*, 70.
- (51) Dyke, J. M.; Groves, A. P.; Morris, A.; Ogden, J. S.; Catarino, M. I.; Dias, A. A.; Oliveira, A. M. S.; Costa, M. L.; Barros, M. T.; Cabral, M. H.; Moutinho, A. M. C. *J. Phys. Chem. A* **1999**, *103*, 8239.
- (52) King, C. M.; Nixon, E. R. *J. Chem. Phys.* **1968**, *48*, 1685.
- (53) Gerakines, P. A.; Moore, M. H.; Hudson, R. L. *Icarus* **2004**, *170*, 202.
- (54) Pettersson, M.; Lundell, J.; Khriachtchev, L.; Rasanen, M. *J. Chem. Phys.* **1998**, *109*, 618.
- (55) Tian, R. J.; Facelli, J. C.; Michl, J. *J. Phys. Chem.* **1988**, *92*, 4073.
- (56) Jamieson, C. S.; Kaiser, R. I. *Chem. Phys. Lett.* **2007**, *440*, 98.
- (57) Hudson, R. L.; Moore, M. H. *Astrophys. J.* **2002**, *568*, 1095.
- (58) Nguyen, M. T.; Sengupta, D.; Ha, T. K. *J. Phys. Chem.* **1996**, *100*, 6499.
- (59) Koch, D. M.; Toubin, C.; Xu, S. C.; Peslherbe, G. H.; Hynes, J. T. *J. Phys. Chem. C* **2007**, *111*, 15026.
- (60) Talbi, D.; Ellinger, Y. *Chem. Phys. Lett.* **1996**, *263*, 385.
- (61) Jamieson, C. S.; Mebel, A. M.; Kaiser, R. I. *Astrophys. J. Suppl. Ser.* **2006**, *163*, 184.
- (62) Palumbo, M. E.; Strazzulla, G. *Astron. Astrophys.* **1993**, *269*, 568.
- (63) Currie, C. L.; Darwent, B. D. *Can. J. Chem.* **1963**, *41*, 1552.
- (64) Larson, C.; Ji, Y.; Samartzis, P. C.; Quinto-Hernandez, A.; Lin, J. J. M.; Ching, T. T.; Chaudhuri, C.; Lee, S. H.; Wodtke, A. M. *J. Phys. Chem. A* **2008**, *112*, 1105.
- (65) Larson, C.; Ji, Y. Y.; Samartzis, P.; Wodtke, A. M.; Lee, S. H.; Lin, J. J. M.; Chaudhuri, C.; Ching, T. T. *J. Chem. Phys.* **2006**, *125*.
- (66) Maier, G.; Lautz, C. *Angew. Chem., Int. Ed.* **1999**, *38*, 2038.
- (67) Drouin, D.; Couture, A. R.; Gauvin, R.; Hovington, P.; Horny, P.; Demers, H. *Monte Carlo Simulation of Electron Trajectory in Solids (CASINO)*, version 2.42; University of Sherbrooke: Sherbrooke, QC, Canada, 2001.
- (68) Mason, N. J.; Dawes, A.; Holtom, P. D.; Mukerji, R. J.; Davis, M. P.; Sivaraman, B.; Kaiser, R. I.; Hoffmann, S. V.; Shaw, D. A. *Faraday Discuss.* **2006**, *133*, 311.
- (69) Bennett, C. J.; Jamieson, C. S.; Osamura, Y.; Kaiser, R. I. *Astrophys. J.* **2006**, *653*, 792.
- (70) Irvine, W. M.; Dickens, J. E.; Lovell, A. J.; Schloerb, F. P.; Senay, M.; Bergin, E. A.; Jewitt, D.; Matthews, H. E. *Earth, Moon, Planets* **1997**, *78*, 29.
- (71) Owen, T. C.; Roush, T. L.; Cruikshank, D. P.; Elliot, J. L.; Young, L. A.; Debergh, C.; Schmitt, B.; Geballe, T. R.; Brown, R. H.; Bartholomew, M. *J. Science* **1993**, *261*, 745.
- (72) Quirico, E.; Doute, S.; Schmitt, B.; de Bergh, C.; Cruikshank, D. P.; Owen, T. C.; Geballe, T. R.; Roush, T. L. *Icarus* **1999**, *139*, 159.
- (73) Johnson, R. E. *Geophys. Res. Lett.* **1989**, *16*, 1233.
- (74) Delitsky, M. L.; Thompson, W. R. *Icarus* **1987**, *70*, 354.
- (75) Lee, T. J.; Rendell, A. P. *Chem. Phys. Lett.* **1991**, *177*, 491.
- (76) Steinfeld, J. I.; Francisco, J. S.; Hase, W. L. *Chemical Kinetics and Dynamics*; Prentice-Hall, Inc.: Upper Saddle River, NJ, 1999.

JP103028V